Available online at www.CivileJournal.org

Civil Engineering Journal

(E-ISSN: 2476-3055; ISSN: 2676-6957)

Vol. 10, No. 03, March, 2024

Eco-friendly 3D Printing Mortar with Low Cement Content: Investigation on Printability and Mechanical Properties

Piti Sukontasukkul [1*], Sila Komkham [1], Sittisak Jamnam [1], Hexin Zhang [2], Kazunori Fujikake [3], Avirut Puttiwongrak [4], Chayanon Hansapinyo [5]

[1] *Construction and Building Materials Research Center, Department of Civil Engineering, Faculty of Engineering, King Mongkut's University of Technology North Bangkok, Bangkok 10800, Thailand.*

[2] *School of Computing, Engineering and the Built Environment, Edinburgh Napier University, Edinburgh EH10 5DT, Scotland, UK.*

[3] *Department of Civil and Environmental Engineering, National Defense Academy, Kanagawa-ken 239-8686, Japan.*

[4] *Geotechnical and Earth Resources Engineering, School of Engineering and Technology, Asian Institute of Technology, Khlong Nueng 12120, Thailand.*

[5] *Department of Civil Engineering, Faculty of Engineering, Chiang Mai University, Chiang Mai 50200, Thailand.*

Received 20 October 2023; Revised 11 February 2024; Accepted 17 February 2024; Published 01 March 2024

Abstract

The conventional approach to achieving optimal printability and buildability in 3D printing mortar relies heavily on cement, which is both costly and environmentally detrimental due to substantial carbon emissions from its production. This study aims to mitigate these issues by investigating the viability of slag as a partial substitute for cement, with the goal of developing an eco-friendly alternative. The newly formulated mortar, featuring a 30% reduction in cement content (from 830 to 581 kg/m3) and the inclusion of 0.10% micro-fibers, exhibits properties comparable to conventional 3D printing mortar. The research is structured into two parts: Part 1 focuses on determining the optimal fiber content, while Part 2 delves into the investigation of fiber-reinforced mortar with reduced cement content for 3D printing. Criteria were established to ensure mortar flow at 115%, initial printable time below 60 minutes, and 7-day compressive strength exceeding 28 MPa. Part 1 results indicate that a fiber content of 0.1% by volume meets the specified requirements. In Part 2, it was observed that increasing the slag replacement percentage extended the initial printable time and time gap. However, even at a 30% replacement rate, the initial printable time remained within the acceptable range, partially attributed to the presence of fibers in the mix. Additionally, higher slag content led to increased flow and reduced filament height in the mixes. Notably, all formulations surpassed the 7-day compressive strength threshold. These findings underscore the potential of slag as a sustainable alternative to cement in 3D printing fiber-reinforced mortar, offering promising prospects for environmentally friendly construction practices.

Keywords: 3D Printing; Eco-friendly Cement Mortar; Slag; Cement Replacement; Printable Cement Mortar; Sustainability Construction.

1. Introduction

In recent years, 3D printing has emerged as a promising technology within the construction industry, offering the potential to enhance efficiency, minimize waste, and enable the fabrication of intricate geometries. However, for widespread adoption of 3D printing, it is imperative to develop materials specifically tailored to this technology. One of the pivotal materials in this context is mortar, which is responsible for forming the structural elements of 3D-printed

* Corresponding author: piti.s@eng.kmutnb.ac.th

http://dx.doi.org/10.28991/CEJ-2024-010-03-010

buildings. The suitability of mortar for 3D printing hinges on several crucial properties [1–3]. Among these, flow is vital, denoting the material's ability to smoothly navigate through the printer nozzle. Printability, another critical attribute, refers to the material's capability to maintain its shape and adhere to the preceding layer upon extrusion. Lastly, buildability is essential, signifying the material's capacity to support subsequent layers' weight without deformation or collapse.

Traditionally, achieving satisfactory buildability and printability in 3D construction mortars involved using substantial proportions of Portland cement, often ranging from 55% to 75% by weight [4]. However, this practice can be costly and environmentally detrimental due to the high carbon emissions associated with cement production [5]. To address this, researchers have explored the use of pozzolan as a partial substitute for cement in 3D printing mortar, aiming to reduce the environmental impact and construction costs. Incorporating pozzolan in 3D printing mortars can have notable effects on both environmental considerations and construction expenses. Firstly, it can diminish the environmental impact by reducing the overall cement consumption, leading to lower carbon emissions and energy consumption during cement production. Secondly, it can lower construction costs by reducing the quantity of cement required for the mortar, presenting a dual advantage for sustainable and economical 3D printing practices.

Nevertheless, utilizing pozzolan as a substitute for cement in mortar for 3D printing yields diverse effects on printability and buildability, contingent on the type and concentration of the pozzolan employed. In the context of fly ash, Panda and Tan [6] replaced cement with fly ash in 3D printing, achieving a replacement rate of up to 80% by mass. They observed that the "ball bearing effect" of fly ash could decrease the yield stress and plastic viscosity of fresh cement composites, enhancing the pumpability of 3D printing. However, at higher replacement rates, there was a delayed initial setting and early hydration, negatively impacting buildability and printability. Rubio et al. [7] discovered that incorporating pozzolans like fly ash (24%) and silica fume (8%) into the mix, instead of replacing cement, increased yield stress, cohesiveness, and improved structure homogeneity and stability, which is advantageous for layer printing. Yet, this did not result in a reduction in cement content since both fly ash and silica fume were additional materials. In summary, while fly ash positively affected cement reduction, workability, cohesiveness, and homogeneity, its major drawback was a slower reaction rate with water, leading to prolonged setting times and lower early-age strength development, adversely affecting buildability.

Concerning ground furnace slag, its use as a substitute for cement in 3D printing mortar seemed to influence the required properties for printable mortar. For instance, Yu et al. [8] determined that slag could replace cement up to 20% by weight without compromising printability and buildability. Their study demonstrated that using up to 10% slag improved the buildability of 3D-printed concrete. However, when the slag content exceeded 20%, a significant deterioration in the rheological properties of 3D-printed concrete and an increase in initial printable time were observed. Xu et al. [9] employed a combination of fly ash/slag (FA/S) and sulfo-aluminate cement (SAC) at various proportions as a partial replacement for cement. They found that with FA content exceeding 20%, there was an increase in slump and a decrease in mechanical properties, affecting buildability. Dai et al. [10] replaced fine aggregate with slag up to 80%, noting that setting time increased gradually with rising FA content, leading to an increase in initial printable time, and both flexural and compressive strengths decreased gradually. However, their study did not result in a decrease in Portland cement content, as slag was used as a fine aggregate replacement rather than a cement replacement.

Problem Statement:

The examination of pozzolanic materials as a substitute for cement in 3D printing mortar, based on the literature review, reveals both positive and negative impacts on its properties. For fly ash, while improvements in flowability, cohesiveness, and homogeneity were noted, the sluggish chemical reaction led to significant delays in setting time and early strength gain. In the case of slag, replacing cement with slag appeared to have fewer adverse effects on initial printable time and early strength gain, but the optimal replacement rate without compromising printable mortar properties was identified at approximately 20%.

Proposed Solution:

This study proposes investigating the use of slag to replace cement in printable mortar up to approximately 30% by weight, aiming to maintain essential properties related to printability and buildability. To address concerns about delayed initial printable time and early strength gain when utilizing slag at percentages exceeding 20%, micro-fibers were introduced into the mix. The presence of micro-fibers in fresh mortar is known to enhance shape and buildability in 3D printing mortar [11–14], as well as reduce the initial printable time [14–15], mitigating the effects of slag replacement. The objective is to develop an eco-friendly mortar that meets the requirements for 3D-printed mortar while significantly reducing cement usage. The cement content in the control mix was set at 830 kg/m^3, and with a 30% replacement, the cement content can be reduced to approximately 581 kg/m^3. Various tests were conducted on the new mortar, focusing on properties such as compressive strength, flow, printability, and buildability. The study's results demonstrate the feasibility of replacing a substantial portion of cement with slag in 3D-printed mortar while still achieving properties that meet the application's requirements.

2. Research Methodology

2.1. Materials

Materials used in this study consisted of (Tables 1 and 2, Figure 1):

- Portland cement Type I with properties that follow the ASTM C150 standard.
- Silica fume with specific gravity of 2.2 and particle size between 0.03-0.30 µm. The chemical composition is given in Table 1.
- Blast furnace slag with specific gravity of 2.9 and particle size of 5.5-7.5 µm. The chemical composition is given in Table 1.
- River sand with particle size passing through sieve no. 16 and specific gravity of 2.5.
- Micro polypropylene fiber with length of 6 mm and diameter between 20-45 µm. Its properties are shown in Table 2.
- Superplasticizer type G – Polycarboxylate base with specific gravity of 1.10.
- Water retention agent – Polyethylene glycol base with specific gravity of 1.09

Table 1. Chemical composition of silica fume and slag

Mineral type (%)	SiO_2	Al_2O_3	Fe_2O_3	CaO	$S0_3$	MgO	Na_2O	K_2O
Silica Fume	88.3	1.2	4.8	0.5	1.1	-	-	-
Slag	32.3	15.4	0.6	39	1.2	7.2	0.7	0.4

Table 2. Properties of micro-polypropylene fiber

Property	Diameter (µm)	Length (mm)	Specific Gravity	Tensile Strength (MPa)	Modulus of Elasticity (MPa)
MFP	25 – 45	6	0.91	650	3445

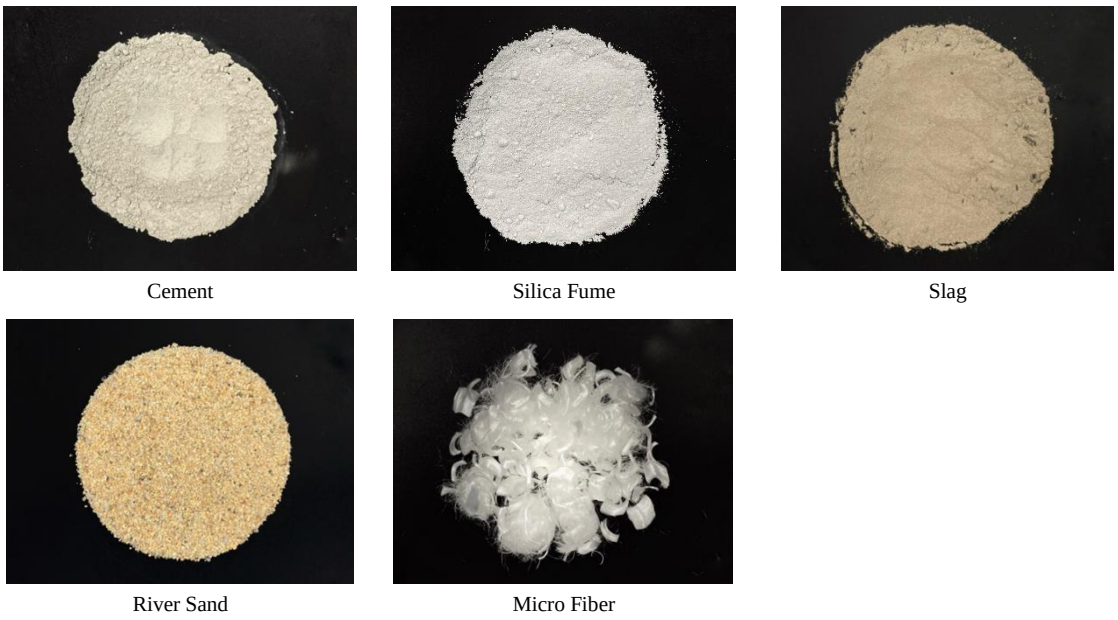

Figure 1. Granular diagram of materials

2.2. Experimental Series

The experimental series comprised two parts:

Part 1: Investigation of the optimum fiber content suitable for 3D printing mortar.

The aim of this study was to determine the optimal volume fraction of fibers that would meet the requirements of mortar for 3D printing applications. As there are currently no standard tests specific to printable cement mortar, the specifications for mortar suitable for 3D printing applications were established based on the property requirements for printable mortar [12]. For example,

- Flow > 115%
- Initial printable time < 60 minutes
- 7-day compressive strength > 28 MPa

The selection of parameters is based on the required performance of printable mortar, including factors such as flowability, printability, and buildability. Initially, cement mortar for 3D printing is in a slurry form, necessitating the ability to flow through a nozzle while maintaining its shape and withstanding pressure from subsequent layers, as well as bonding with the previous layer. Parameters were established to meet these requirements. For instance, a flow of 115% was set as the flowability requirement, while the initial printable time of 60 minutes ensures uniform extrusion without defects, aligning with printability needs. This time frame is derived from the standard concrete mixing-to-placing duration of 60 minutes to prevent stiffness. Compressive strength requirements ensure the mortar can withstand loads after 7 days. Buildability, though not initially defined, is evaluated later based on the time gap established to prevent vertical deformation during the printing of up to 10 layers. This approach ensures the stack of mortar filaments remains virtually free of vertical deformation.

The mix proportion meeting these 3D printing specifications was chosen to undergo further investigation in Part 2.

Part 2: Investigation on fiber reinforced mortar with low cement content for 3D printing.

The purpose of this test was to produce printable mortar with reduced Portland cement content while maintaining its properties and meeting the printability requirements for 3D printing mortar outlined in Part 1. The Portland cement content of the mix proportion selected from Part 1 was substituted with slag at weight percentages ranging from 0% to 30% of the cement weight. The proportions of river sand, silica fume, water, and water retention agents remained constant. However, as the addition of slag significantly impacted the workability of the mortar, the superplasticizer dosage for each mix proportion had to be predetermined to ensure sufficient flowability suitable for printing. Subsequently, the proposed mix proportions underwent printability tests to assess the initial printable time, time gap, and layer deformation (10 layers). Mechanical property was also conducted to evaluate the effect of slag replacement. The research sequence is summarized in Figure 2.

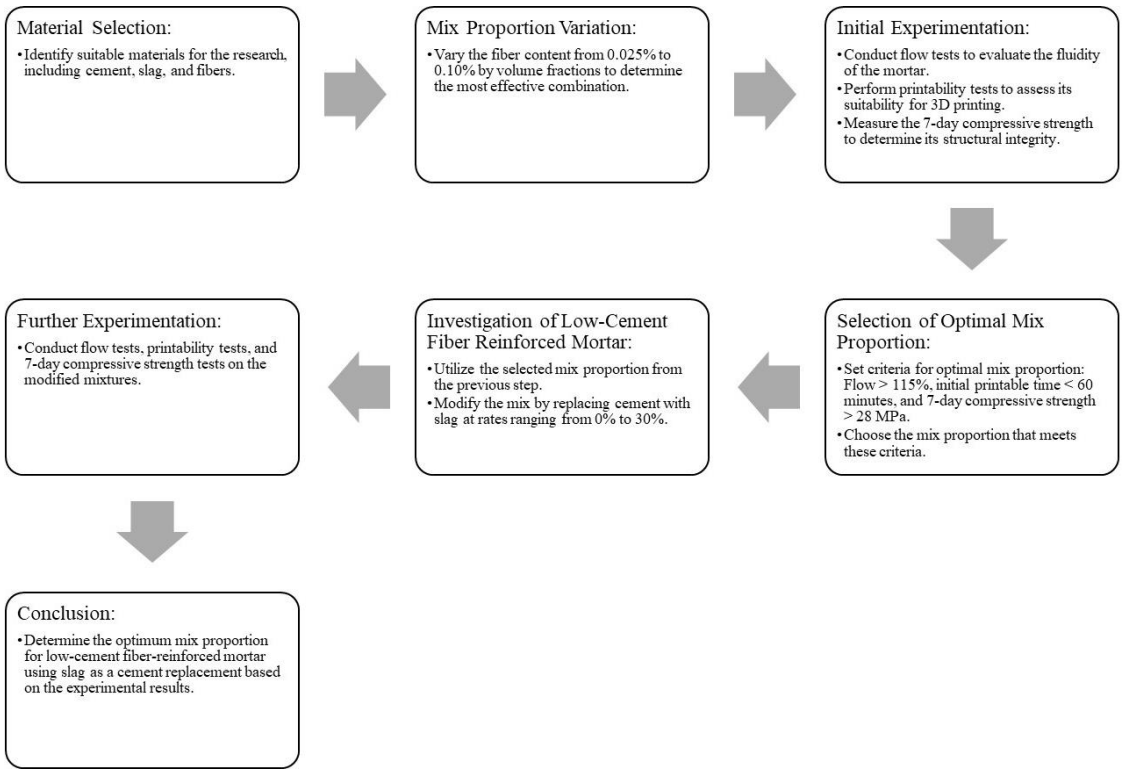

Figure 2. Schematic illustration of research sequence

2.3. Mix Proportions

For Part 1, the mix proportion primarily comprised cement, silica fume, river sand, and admixtures. The fiber content ranged from 0% to 0.1% by volume. In the control mix (plain mortar, PLN), the proportions were cement at 878 kg/m³, river sand at 1170 kg/m³, silica fume at 88 kg/m³, and water at 212 kg/m³. The superplasticizer and water retention agent were fixed at 10.0% and 2.5% by weight of the binder, respectively. In the fiber-reinforced cement mortar (FRM), the fiber content varied from 0%, 0.025%, 0.050%, 0.075%, to 0.100% by volume (PLN, FRM25, FRM50, FRM75, and PP100). Detailed mix proportions are provided in Table 3.

Table 3. Detailed mix proportion for Part 1

Specimen type	Materials (kg/m^3)						
	Portland cement	Sand	Silica Fume	Water	Super plasticizer	PEG	Micro fiber
PLN	830	1170	165	212	97	24	0
FRM25							0.23
FRM50							0.45
FRM75							0.68
FRM100							0.91

For Part 2, the mix proportion selected from Part 1, which met the earlier mentioned requirements in 2.2, was utilized. The cement content was replaced with slag at rates ranging from 0% to 30% of the cement weight. Other components, including river sand, silica fume, fiber, and water content, remained constant. However, to maintain consistent workability, the optimal superplasticizer content, resulting in a flow of 115%, was determined and applied to each mix proportion. Detailed mix proportions are provided later in the experimental section after determining the optimal fiber content from Part 1.

2.4. Experimental Series

2.4.1. Flow Table Test

The test was conducted in accordance with ASTM C230 (Standard Specifications for Flow Table for Use in Tests of Hydraulic Cement). It commenced with placing an inverted cone container on the flow table and filling it with fresh cement mortar. Gradually lifting the container allowed the fresh mortar to flow and spread slightly on the flow table. Subsequently, the face of the table was raised and dropped freely 15 times, further spreading the fresh mortar. The flow diameter (D1) was determined as the average measurement of the maximum flow diameter observed at least twice. The flow percentage can then be calculated using Equation 1.

$$Flow\ (\%) = \frac{D_1 - D_0}{D_0} \times 100 \quad (1)$$

where D_0 is the original diameter (mm), D_1 is the diameter after impact (mm).

2.4.2. Printable Time

Printable time refers to the duration during which a material can be printed continuously without defects while maintaining consistent dimensional lines. It commences with the initial printable time (t_{int}) and concludes with the final printable time (t_{fin}). In the experiment, a 3D printer, designed and constructed at the Department of Civil Engineering, KMUTNB (Figure 3), was utilized to print 300 mm filaments of mortar every 5 minutes until printing was no longer feasible. The printer featured a 20 mm diameter nozzle, operated at a height of 15 mm above the floor, moved at a speed of 10 mm/s, and maintained a feed rate of 2.5 ml/s. The width of each filament was measured at 50-, 150-, and 250-mm intervals, and the average of these values represented the width (Figure 4). Results were graphed against time, illustrating changes in filament width due to the diminishing plasticity of fresh mortar over time (Figure 5). The initial printable time was recorded when the filament consistently reached its narrowest width, and the final printable time was noted when printing became inconsistent. The dimension of the filament printed at the initial printable time is referred to as the initial dimension, consisting of the initial width (w_{int}) and initial height (h_{int}).

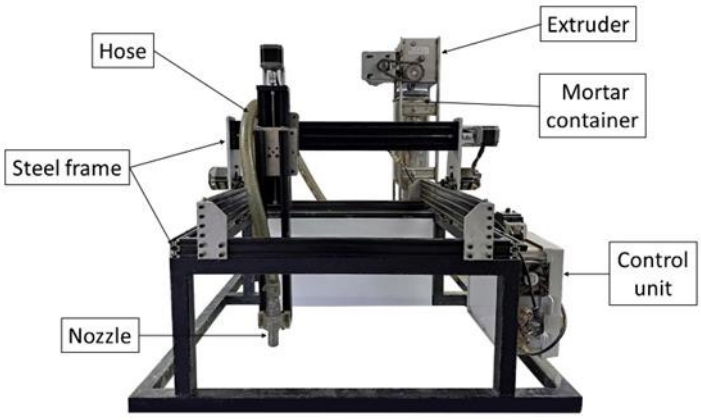

Figure 3. Small scale 3D printer

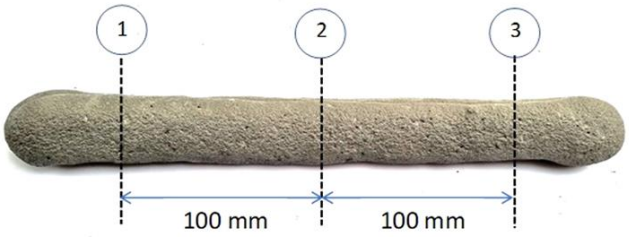

Figure 4. Width measurement location

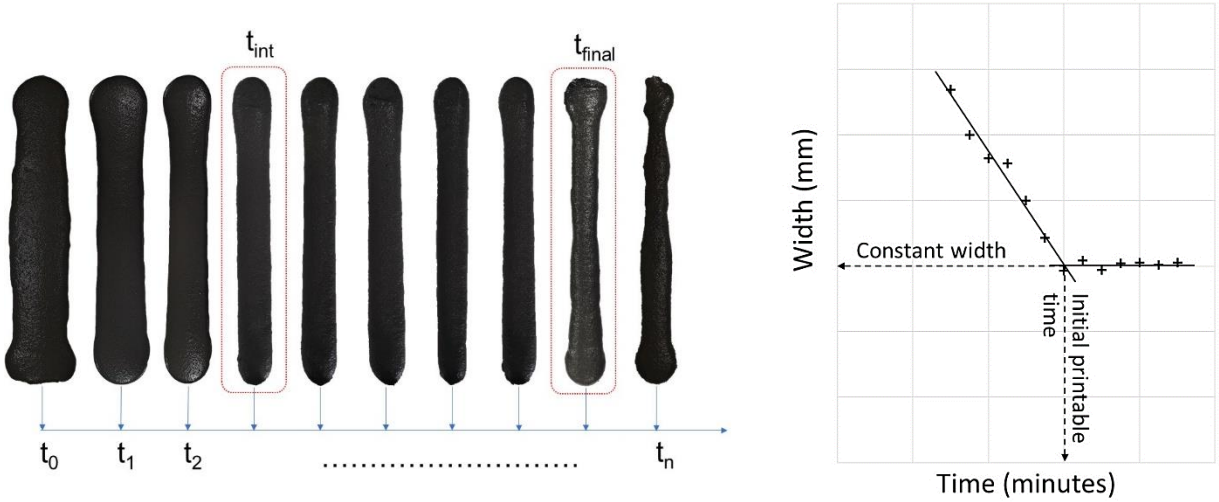

Figure 5. Relationship between filament width vs time

2.4.3. Time Gap without Layer Deformation

In this study, the term "time gap" denotes the duration between printing the first layer and subsequent layers without causing any deformation to the first layer. To assess this, the initial printable time obtained from section 2.4.3 was used to print the first layer. Five minutes later, a print filament was added on top of the first layer, and the deformation of the first layer was promptly measured. This process was repeated at five-minute intervals until no deformation was observed in the first layer. The earliest time at which the first layer no longer deformed is referred to as the "time gap without deformation."

The purpose of this test was to evaluate the buildability property of fresh mortar, or its ability to support weights of subsequent layers without deformation. This property can be linked to a specific time after the cement comes into contact with water. The obtained time gap was validated by printing 10 layers of each mix proportion, measuring their height, and comparing them with the expected height (which is equal to 10 times the hint). If the actual height of the 10 printed layers falls within the expected height range, it can be concluded that the obtained time gap was sufficient to prevent deformation of the previous layer during printing.

2.4.4. Mechanical Properties

Two tests were conducted, namely a compressive strength test (ASTM C109) and a flexural strength test (ASTM C348-21). As these tests are widely performed and well-established globally, detailed test procedures have been omitted from this manuscript. However, specifications regarding specimen types and test directions are provided instead.

Two types of specimens underwent both tests: cast and printed specimens. Cast specimens were cast with dimensions of 50×50×50 mm for compressive strength testing and 40×40×160 mm for flexural strength testing. These specimens were prepared in accordance with the corresponding standard and wrapped in plastic sheeting until the test date (7 days).

For printed specimens, they were printed in a prism shape, wrapped, and cured for 7 days. Subsequently, they were cut and polished into shapes similar to the cast specimens (Figure 6). To investigate the effect of load directions on printed specimens, the following test schemes were proposed:

- For the compression test, two load directions were proposed: perpendicular to and parallel to the print direction (Figure 7-a).
- For the flexure test, two load directions were applied: perpendicular to and transverse to the print direction (Figure 7-b).

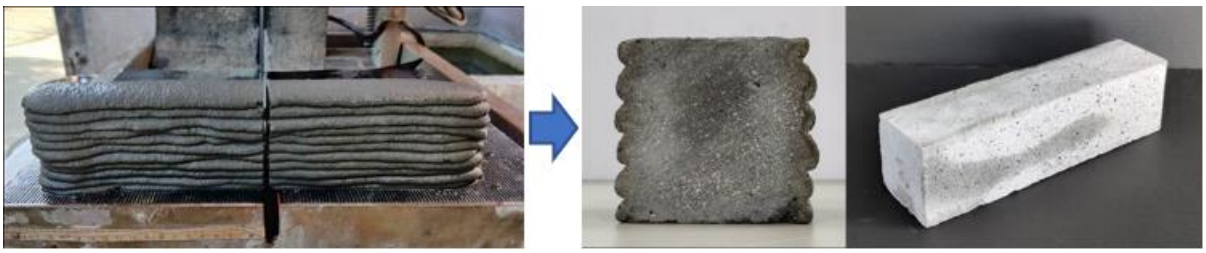

Figure 6. Preparation of printed specimens for compression and flexure testing

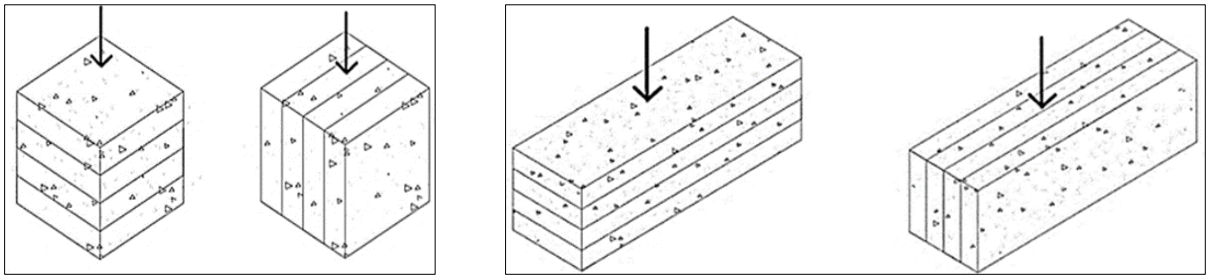

(a) (b)

Figure 7. Load directions vs. specimen layout for (a) compression and (b) flexure testing

3. Results and Discussion

3.1. Part 1

3.1.1. Flow Test

The flow percentage of fiber-reinforced mortar for 3D printing was determined through the flow test in accordance with ASTM C230, and the results are presented in Figure 8. It was observed that the flow rate decreased as the micro polypropylene fiber content increased. This phenomenon was attributed to the increased surface area of the microfibers, which absorbed water from the mix, thereby reducing the free water content and hindering the mobility of the fresh cement mortar. Additionally, the formation of a fiber interlocking network can increase the viscosity of the mortar, making it thicker and more resistant to flow [16]. FRM100 exhibited the lowest flow rate of 129%, which was 14% lower than that of the PLN mixture. These results align with the findings of Guerini et al. [17], who reported a decrease in the workability of concrete with increasing fiber content from 0.5% to 1.0%. Similarly, Dai et al. [18] reported a decrease in flowability with an increase in waste plastic fiber content from 0.1% to 0.7%. They suspected that the dispersion of fibers prevented the contact between water and cement particles, resulting in reduced flowability.

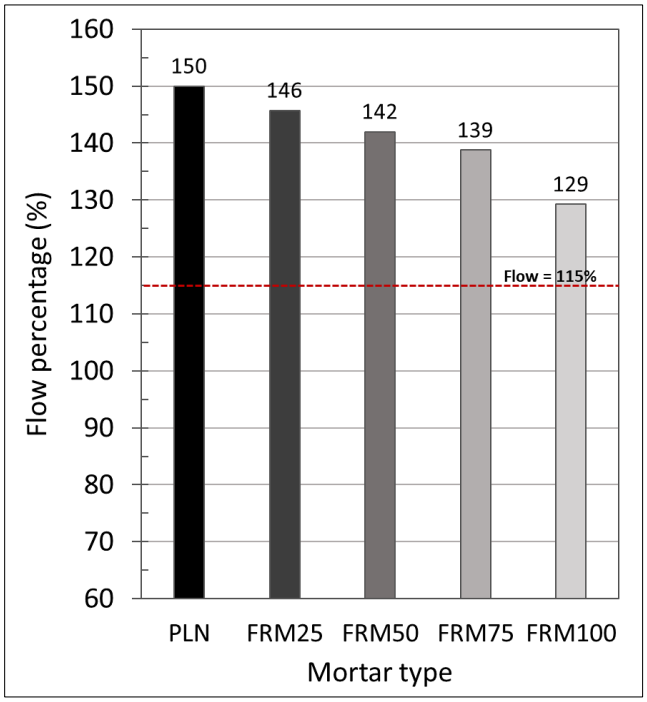

Figure 8. Flow percentage

All mix proportions tested in this study met the required flow criteria for 3D printing application, as they exhibited a flow percentage higher than 115%.

3.1.2. Initial Printable Time (T_{int})

Figures 9 depict the correlation between filament width and time. From the plotted results, the initial printable time of each mix can be calculated, as shown in Table 4. Typically, T_{int} decreases with an increase in fiber content. The highest T_{int} of 67.5 minutes was observed for plain mortar (PLN). On the other hand, the T_{int} for FRM ranged from 53-63 minutes and was lower than that of PLN. FRM100 exhibited the lowest initial printable time of 53 minutes. The addition of microfiber increased the total specific surface area of the mortar mix, necessitating more water and resulting in a lower water/cement ratio, which caused the mortar to set faster. Additionally, the addition of fibers increased the solid content of the mix, providing support to the fresh mix and allowing it to gain dimensional stability more quickly. The addition of microfiber to the mortar results in a reduction in flow, leading to increased stability of the filaments. This decrease in flow translates to a lower initial printable time, enabling FRM to commence printing more rapidly.

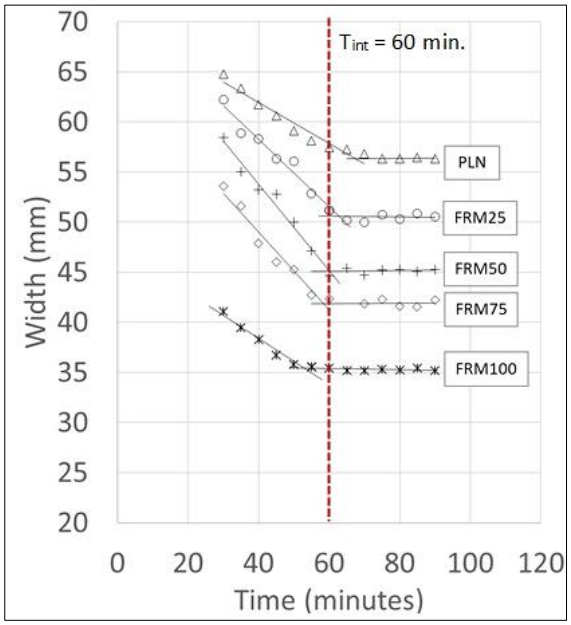

Figure 9. Filament width vs. time of plain and FRM

Table 4 illustrates the correlation between initial filament width (W_{int}) and initial printable time (T_{int}) for each mix. Wint ranges from 35 to 56 mm, with the widest width of 56 mm observed in plain mortar (PLN). The addition of fiber narrows Wint, signifying that fibers offer support to the printed filament and minimize vertical deformation. The smallest width of 35.4 mm was observed in FRM100. The initial height of the filament (H_{int}) increases with the addition of fiber, attributed to the constant volume of mortar extruded through the nozzle. Fibers reinforce the mortar matrix, providing additional structural support to the printed filaments, thus preventing deformation or sagging during printing and enhancing stability [19].

Table 4. Effect of fiber content on initial printable time and filament dimension

Concrete Type	Initial Printable time (minutes)	Width (mm)	Height (mm)
PP0	67.5	56.3	6.0
PP25	62.7	50.6	6.6
PP50	60.2	45.1	7.5
PP75	58.4	41.9	8.2
PP100	53.0	35.4	9.7

The relationship between height and time indicates that Hint increases over time, plateauing once the Tint is achieved, and height increases with fiber content. The shortest filament height of 6 mm was observed in the PLN mix, while the tallest of 9.7 mm was seen in the FRM100 mix. The enhanced stability provided by fibers enables printing of taller filaments without risk of collapse or deformation, allowing for greater height while maintaining structural integrity [20].

3.1.3. 7-day Compressive Strength

Figure 10 illustrates the compressive strength results of printed specimens tested with loads perpendicular and parallel to the print direction. The data demonstrates that the compressive strength of printed mortar increases with higher fiber content, irrespective of load direction. The addition of microfibers enhances bonding between particles and aggregates, reinforces the matrix, mitigates cracks by bridging microcracks, and increases toughness, improving load distribution and deformation resistance. This reinforcement enhances cohesion, restricts crack propagation, and enhances the mortar's capacity to withstand loads, leading to higher compressive strength [21]. The FRM100 mix exhibited the highest compressive strength values in both load directions (28.3 MPa perpendicular and 21.9 MPa parallel to print direction), while the PLN mix showed the lowest values (23.9 MPa perpendicular and 16.3 MPa parallel to print direction). Similar findings on the fiber's strengthening effect were reported by Sukontasukkul et al. [14, 15] and Panda et al. [22], where increased fiber content correlated with higher strength, potentially due to enhanced interlayer bond strength between printed layers.

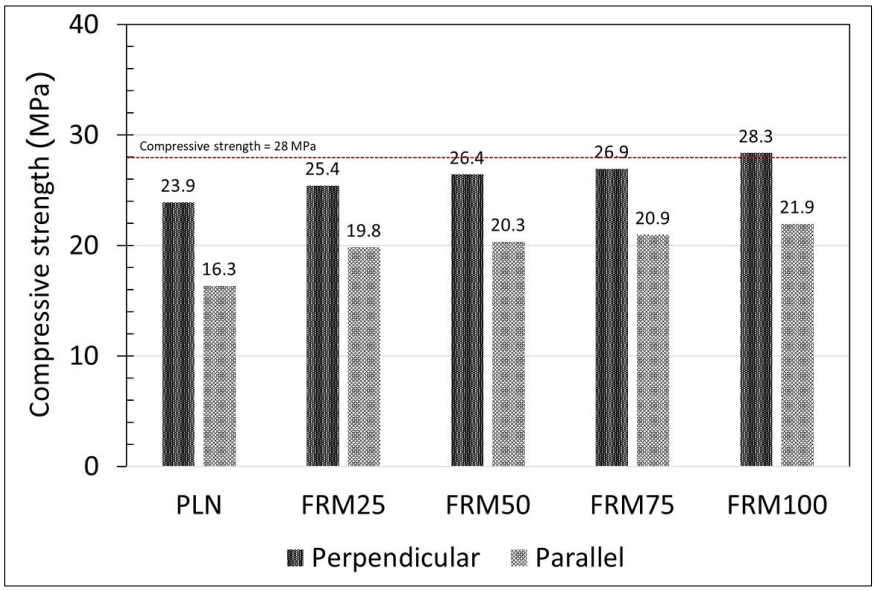

Figure 10. Compressive strength of printed specimen tested in perpendicular and parallel directions

In comparing print direction to load direction, higher compressive strength values were observed for the load direction perpendicular to the print direction compared to the load direction parallel to the print direction. This disparity in compressive strength could be attributed to the debonding between print layers and the weaker interlocking effect of fibers in the parallel load direction (Figure 11). This finding is consistent with research by Paul et al. [22] and Dai et al. [23], which suggests that layer-by-layer printing creates weaker bonds within specimens, resulting in reduced load-carrying capacity under compressive, tensile, and flexural loads, necessitating stress transfer across or along these layers. Studies by Ding et al. [24] and Ma et al. [25] further support this observation, highlighting the high anisotropic behavior of 3D printed specimens under different loading directions. Mechanical properties are significantly influenced by load and print directions. Additionally, the data indicates that fiber reinforcement can enhance the compressive strength of printed mortar, emphasizing the potential of fiber-reinforced mortar for 3D printing applications.

(a) (b)

Figure 11. Failure patterns of specimens tested with load (a) parallel and (b) perpendicular to print direction

Based on the test results from flow, initial printable time, and compressive strength at 7 days, and the criteria for mix proportion selection, the FRM100 which exhibited flow of 129% (>115%), initial printable time of 53 minutes (< 60 min.), and 7-day compressive strength of 28.3 MPa (>28 MPa) was selected to continue further investigation in Part 2.

3.2. Part 2: Investigation on Fiber Reinforced Mortar with Low Cement Content for 3D Printing

3.2.1. Mix Proportions Selection based on Flow Test

In this phase of the study, as detailed in section 3.1.3, the cement content of FRM100 was substituted with slag at weight percentages of 10%, 20%, and 30%, resulting in a notable reduction in cement content from 830 to 581 kg/m^3. However, this substantial replacement of slag altered the rheological properties of the mortar, leading to a significant increase in flow (refer to Figure 10). The increased flow of concrete with the use of slag can be attributed to several factors. Firstly, slag consists of finer particles compared to cement, which enhances particle packing and lubrication within the concrete mixture, enabling improved flowability. Moreover, slag can act as a water reducer, allowing for a reduction in water content while maintaining desired workability, leading to improved flow. Lastly, the incorporation of slag can improve the rheological properties of concrete by enhancing viscosity and yield stress, promoting better flow without segregation or bleeding. These factors contribute to the enhanced flow of concrete when slag is used as a supplementary material [26, 27].

The experiment began by adjusting the superplasticizer content of each mix proportion within the range of 5% to 10%, followed by a flow test. The correlation between flow and superplasticizer content was then determined and illustrated in Figure 12. Analysis of the results revealed that, for equivalent superplasticizer content, flow increased proportionally with the amount of slag replacement. Consequently, to sustain a flow rate of 115%, adjustments were required in the superplasticizer dosage, reducing it from 7.3% to 6.3%, 5.8%, and 5.4% with slag replacement rates of 0%, 10%, 20%, and 30%, respectively. Refer to Table 5 for detailed mix proportions pertaining to Part 2.

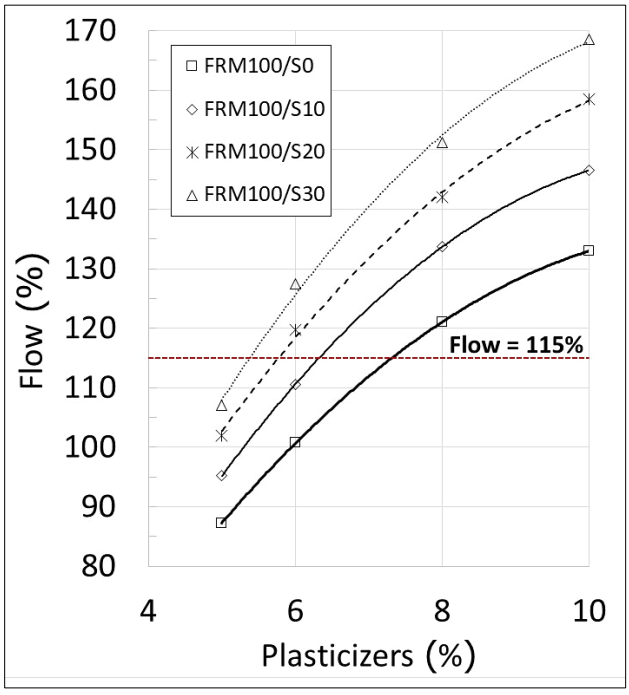

Figure 12. Relationship between flow and superplasticizer of FRM100 with slag replacement

Table 5. Detailed mix proportion for Part 2

Specimen type	Materials (kg/m^3)							Super Plasticizer (%)
	Portland cement	Sand	Silica Fume	Water	PEG	Micro fiber	Slag	
FRM100/S0	830	1170	165	٢١٢	24	0.91	0	7.3
FRM100/S10	747						83	6.3
FRM100/S20	664						166	5.8
FRM100/S30	581						249	5.4

3.2.2. Initial Printable Time

Figure 13-a illustrates the outcomes of the experiment, showcasing the correlation between filament width and time. It was observed that the filament width exhibited an increasing trend with the slag replacement rate, regardless of the printing time. This phenomenon can be attributed to the heightened flow characteristics of FRM with slag replacement (FRM/S), resulting in broader filament widths while simultaneously shortening the height, as expounded in section 3.2.1.

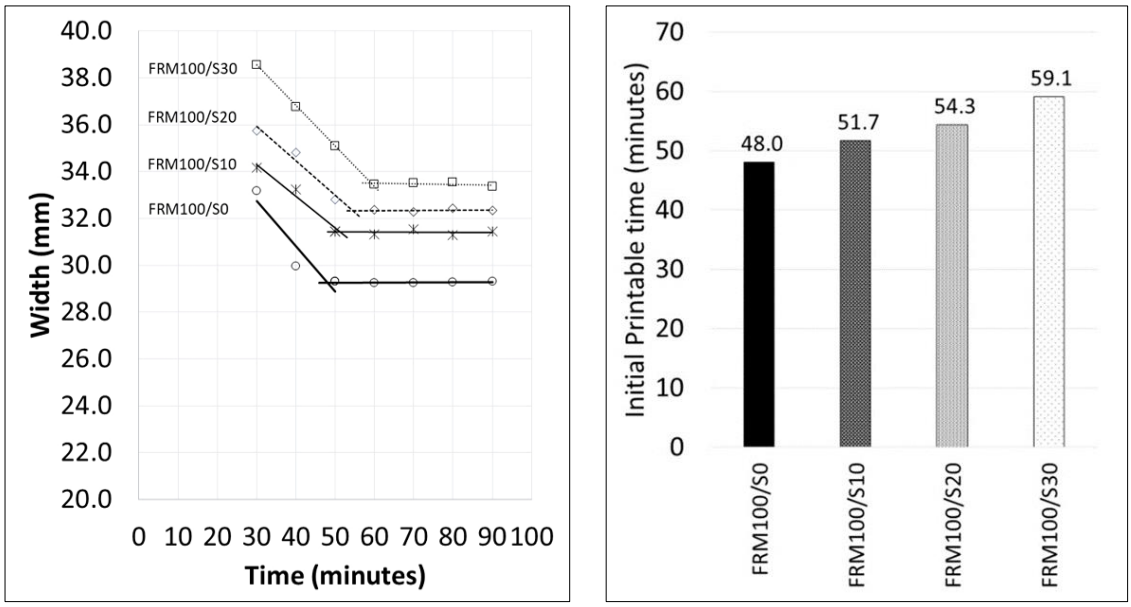

(a) (b)

Figure 13. (a) Relationship between filament width vs. time and (b) Initial printable time

The initial printable time (t_{int}) represents the duration during which the mortar can be continuously printed at a consistently narrow width. As depicted in Figure 13-b, the tint values were determined from the filament width-time relationship. The results revealed a noticeable increase in tint from 48 to 59 minutes with the escalation of the slag replacement ratio from 0% to 30%. This decline in tint can be attributed to the reduction in cement content, which decelerates the hydration reaction rate and subsequently impacts the mortar's uniform printing ability, thereby prolonging the tint. Despite the rise in t_{int} associated with increasing slag replacement rates, all mix proportions with slag replacement up to 30% remained within the stipulated requirement of less than 60 minutes.

The increase in initial printable time related to higher slag content implies that mortar with a higher slag ratio demands a longer waiting period compared to conventional mortar, possibly causing delays in construction timelines. However, the presence of microfiber offers a mitigating factor, as it has been shown to reduce t_{int}. Consequently, the incorporation of microfiber can offset the increase in t_{int} induced by higher slag content, effectively maintaining it below the critical threshold of 60 minutes. This synergistic effect between microfiber and slag content underscores their combined potential in optimizing construction efficiency and overcoming challenges posed by extended waiting periods, thereby enhancing the feasibility of utilizing slag-based mortar in 3D printing applications.

The initial width (w_{int}) and height (h_{int}) were determined by measuring the dimensions of the printed filaments at their respective initial printable times. Three measurements were taken at different positions along each filament, with at least three filaments printed for each mortar type. The average value of these measurements was then calculated to represent each mortar type. The results are outlined in Table 6. It is evident that as the slag replacement ratio increases, the initial width (w_{int}) of the filaments also increases, ranging from 29.3 mm for FRM100/S0 to 33.5 mm for FRM100/S30. This indicates a reduction in mortar viscosity with increasing slag content. Conversely, the height decreases from 12.7 mm for FRM100/S0 to 10.8 mm for FRM100/S30. This phenomenon suggests that with a constant volume of mortar extruded from the nozzle, the broader width results in a shorter height

Table 6. Initial printable time, width, and height

Mortar Type	t_{int}	w_{int}	h_{int}
FRM100/S0	48.0	29.3	12.7
FRM100/S10	51.7	31.4	11.7
FRM100/S20	54.3	32.3	11.2
FRM100/S30	59.1	33.5	10.8

3.2.3. Time Gap

Table 7 presents the results regarding the correlation between slag replacement rate and parameters, including time gap, expected height, and actual height attained during printing. The time gap signifies the duration between printing the initial layer and subsequent layers without inducing any deformation to the first layer. Expected height refers to the anticipated height after printing 10 layers of each mix proportion (10 x h_{int}), while actual height denotes the height obtained from printing 10 layers of each mix proportion.

Table 7. Time gap, expected height, and actual height

Mortar type	Time gap (min)	Expected height (mm)	Actual height (mm)	Difference (mm)
FRM100/S0	8	127	127.6	-0.60
FRM100/S10	8	117	117.3	-0.30
FRM100/S20	12	112	111.9	0.10
FRM100/S30	13	108	107.7	0.30

As the slag replacement ratio escalates from 0% to 30%, the time gap increases by 62.5% (from 8 minutes to 13 minutes). This implies that incorporating slag as a partial cement substitute prolongs the time gap before the first layer experiences deformation. This trend can be attributed to the slower setting of mortar with higher slag content, allowing an extended working duration before it stiffens too much for additional layering.

Moreover, the data reveals a decrease in actual height with an increasing slag replacement rate, aligning with the findings in section 3.2.2 where initial height decreases with higher slag replacement rates. Additionally, the actual height falls within a similar range to the expected height for all mix proportions, exhibiting differences ranging from 0.24% to 0.97%. This highlights the appropriateness of the attained time gap in avoiding deformation of preceding layers during printing, thereby preserving the structural integrity of the printed objects. Despite elongating the time gap, incorporating slag as a partial cement substitute up to 30%, coupled with fiber addition, maintains the required buildability characteristic of fresh mortar, with minimal deformation of the initial layer. A similar observation by Li et al. [28] highlights that fiber addition (glass) enhances dimensional stability in printed filaments, imparting practical implications for printing intricate geometries or large-scale structures.

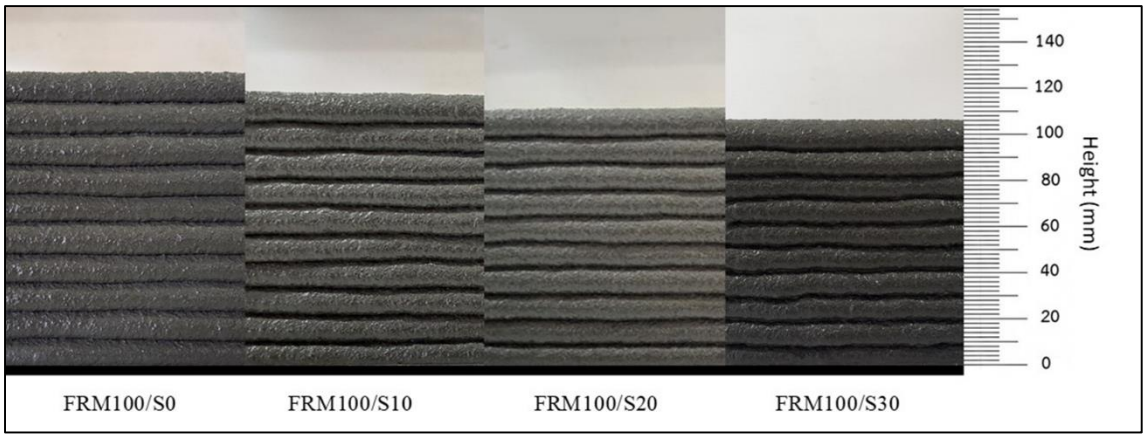

Figure 14. Actual printed height (10 layer) of FRM with slag replacement

3.2.4. Mechanical Properties

3.2.4.1. 7-day Compressive Strength

Figure 15 depicts the compressive strength of mortar with varying slag replacement ratios under two loading directions: perpendicular and parallel to the print direction. Initially, it is evident that as the slag replacement ratio increases, the compressive strength values improve in both loading directions. This enhancement can be attributed to the finer particles introduced by slag, which enhance packing and consequently bolster strength [27]. Additionally, the increased slag content fosters pozzolanic reactions, wherein it reacts with calcium hydroxide in the presence of water to form additional cementitious compounds, augmenting overall strength [29].

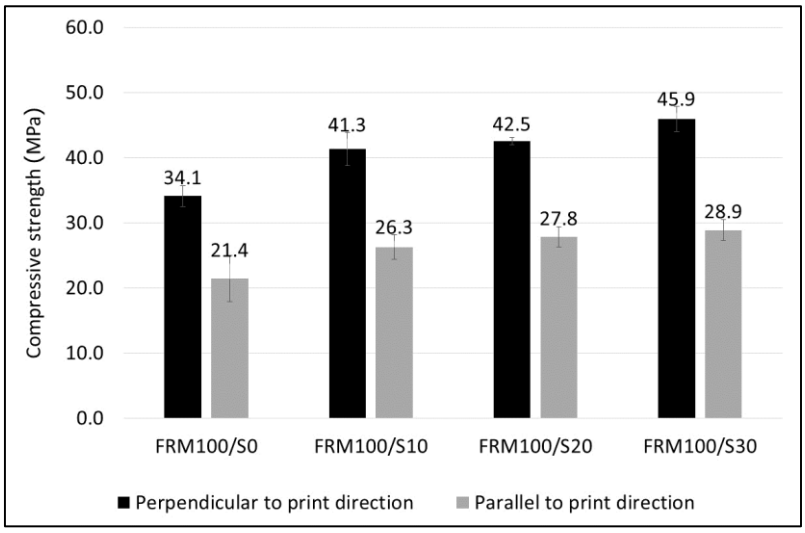

Figure 15. 7-day Compressive strength of FRM with slag replacement

Comparing the compressive strength values between perpendicular and parallel loading directions reveals a noteworthy disparity. Compressive strength in the perpendicular direction consistently surpasses that in the parallel direction for all slag replacement ratios. This discrepancy is attributed to the layer-by-layer printing process, which results in weaker bonding between adjacent layers in the parallel direction, thus yielding lower compressive strength. Conversely, the perpendicular direction benefits from interlocking between layers, bolstering compressive strength. Shakor et al. [30] underscored the significant influence of orientation angle on the mechanical properties of printed specimens, noting that optimal strength is achieved with specific printing orientations. Furthermore, within the perpendicular direction, compressive strength increases with higher slag replacement ratios, with FRM100/S30 exhibiting the highest strength. This can be attributed to the denser and more compact mortar achieved with increased slag content.

In summary, incorporating slag as a partial cement replacement enhances the compressive strength of printed mortar in both loading directions, with a more pronounced effect in the perpendicular direction. Moreover, higher slag replacement ratios correlate with greater strength gains. While most mortar types meet or exceed the 7-day compressive strength requirement (>28 MPa) in the perpendicular direction, only FRM100S30 achieves this threshold in the parallel direction.

3.2.4.2. 7-day Flexural Strength

The data provided shows the flexural strength of four different types of mortar with varying slag replacement ratios, tested with loads perpendicular and transverse to the print direction.

From the data, it can be observed that the flexural strength increases with increasing slag replacement ratio for both perpendicular and transverse loads. The flexural strength increases range from 20.5% to 25.2% for the perpendicular and transverse directions, respectively, when comparing 30% slag replacement to 0% slag replacement (Figure 16). This trend indicates that the use of slag as a partial cement replacement can improve the flexural strength of the printed objects.

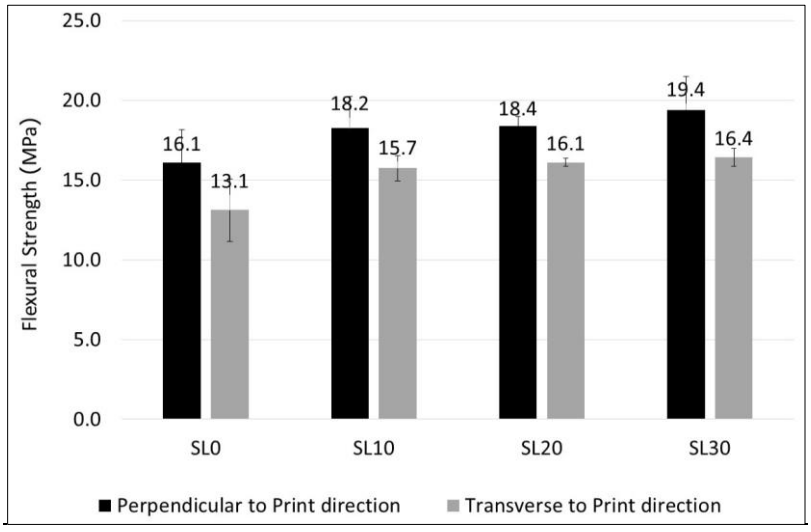

Figure 16. 7-day Flexural strength of FRM with slag replacement

Furthermore, it can be observed that the flexural strength values in the perpendicular direction consistently exceed those in the transverse direction for all mortar mixtures. This may be attributed to a combination of factors, including the layer-by-layer printing process which may result in weaker bonding between adjacent layers in the transverse direction and the expansion of the material in the transverse direction due to Poisson's effect which lead to debonding and to lower flexural strength. Shakor et al. [30] used ABAQUS to simulate the deflection of 3D printing beam subjected to load in different directions. They also found that when load was acting in perpendicular to the print direction, the beam exhibited the lowest deflection and hence, yielded the highest flexural strength.

The test results indicating higher flexural strength for specimens tested with load perpendicular to the print direction compared to those tested with load transverse to the print direction suggest important considerations for practical applications of 3D printed structures. This finding implies that the orientation of the printed structure relative to the applied load can significantly influence its strength and structural integrity. Therefore, in real-world applications, designers and engineers should carefully consider the orientation of 3D printed components to ensure optimal strength and performance.

Overall, the results suggest that the use of slag as a partial cement replacement can improve the flexural strength of 3D-printed objects and that the flexural strength is generally higher in the perpendicular direction compared to the transverse direction.

4. Conclusions

The conclusion can be divided into two parts:

Part 1: This section explores the impact of micro polypropylene fibers on the flow percentage, initial printable time, and compressive strength of fiber-reinforced mortar (FRM) for 3D printing. Results indicate that the addition of fibers decreased the flow rate due to increased surface area and water absorption. However, all mix proportions met the required flow criteria for 3D printing (115%). Moreover, the initial printable time decreased with an increase in fiber content, suggesting that fibers provide support to the fresh mix, enabling quicker dimensional stability. Among the FRM mixes, FRM75 and FRM100 met the 60-minute t_{int} requirement. Compressive strength increased with fiber content, with only FRM100 exhibiting a compressive strength higher than 28 MPa. Based on its flow, initial printable time, and compressive strength results, FRM100 was selected for further investigation on printable mortars with low cement content.

Part 2: This segment explores the effect of slag as a partial cement replacement on the rheological and mechanical properties of FRM. The replacement of cement content with slag at weight percentages of 10%, 20%, and 30% led to a significant reduction in cement content from 830 to 581 kg/m^3. However, the rheological properties of the mortar were notably affected by the slag replacement, necessitating adjustments to the superplasticizer to maintain a consistent flow of 115%. Although decreasing cement content increased the initial printable time, all mix proportions with slag replacement up to 30% remained within the required limit, partially attributed to the presence of fibers in the mix. The use of slag as a partial cement replacement influenced the initial dimensions of the printed filaments, resulting in increased filament width and shorter filament height due to higher flowability. Moreover, compressive and flexural strengths increased with slag replacement. However, both flexural strengths appeared to be dependent on the direction of load vs. the printing direction in which the perpendicular strength exceeding the parallel strength (or transverse in the case of flexural strength). Overall, this investigation suggests that using slag as a partial cement replacement up to 30% is feasible for reducing the cement content of FRM for 3D printing while maintaining workability and initial printable time and enhancing both compressive and flexural strengths.

While parameters related to printing configuration, such as nozzle shape, size, printing speed, and layer thickness, require further investigation, we recommend exploring these factors in future studies.

5. Declarations

5.1. Author Contributions

Conceptualization, P.S. and S.K.; methodology, P.S. and S.K.; validation, S.J., H.Z., K.F., A.P., and C.H.; formal analysis, S.K.; investigation, S.K.; resources, P.S.; data curation, S.K.; writing—original draft preparation, P.S., H.Z., and S.J.; writing—review and editing, P.S., H.Z., K.F., and C.H.; visualization, S.K.; supervision, P.S.; project administration, P.S.; funding acquisition, P.S. All authors have read and agreed to the published version of the manuscript.

5.2. Data Availability Statement

The data presented in this study are available on request from the corresponding author.

5.3. Funding

This research is funded by the National Research Council of Thailand (NRCT), and the National Science, Research and Innovation Fund (NSRF) and King Mongkut's University of Technology North Bangkok (KMUTNB) under the contract no. KMUTNB-FF-66-02.

5.4. Acknowledgements

The authors gratefully acknowledge Ruth Saints from Edinburgh Napier University for proofreading the manuscript. Additionally, appreciation is extended to the Science, Technology, and Research Institute (STRI) at KMUTNB for their support in funding acquisition.

5.5. Conflicts of Interest

The authors declare no conflict of interest.

6. References

[1] Buswell, R. A., Leal de Silva, W. R., Jones, S. Z., & Dirrenberger, J. (2018). 3D printing using concrete extrusion: A roadmap for research. Cement and Concrete Research, 112, 37–49. doi:10.1016/j.cemconres.2018.05.006.

[2] Saruhan, V., Keskinateş, M., & Felekoğlu, B. (2022). A comprehensive review on fresh state rheological properties of extrusion mortars designed for 3D printing applications. Construction and Building Materials, 337, 127629. doi:10.1016/j.conbuildmat.2022.127629.

[3] Zhang, J., Wang, J., Dong, S., Yu, X., & Han, B. (2019). A review of the current progress and application of 3D printed concrete. Composites Part A: Applied Science and Manufacturing, 125, 105533. doi:10.1016/j.compositesa.2019.105533.

[4] Beersaerts, G., Hertel, T., Lucas, S., & Pontikes, Y. (2023). Promoting the use of Fe-rich slag in construction: Development of a hybrid binder for 3D printing. Cement and Concrete Composites, 138, 104959. doi:10.1016/j.cemconcomp.2023.104959.

[5] Dey, D., Srinivas, D., Panda, B., Suraneni, P., & Sitharam, T. G. (2022). Use of industrial waste materials for 3D printing of sustainable concrete: A review. Journal of Cleaner Production, 340, 130749. doi:10.1016/j.jclepro.2022.130749.

[6] Panda, B., & Tan, M. J. (2019). Rheological behavior of high volume fly ash mixtures containing micro silica for digital construction application. Materials Letters, 237, 348–351. doi:10.1016/j.matlet.2018.11.131.

[7] Rubio, M., Sonebi, M., & Amziane, S. (2017). 3D printing of fibre cement-based materials: fresh and rheological performances. Academic Journal of Civil Engineering, 35(2), 480-488. doi:10.26168/icbbm2017.74.

[8] Yu, Q., Zhu, B., Li, X., Meng, L., Cai, J., Zhang, Y., & Pan, J. (2023). Investigation of the rheological and mechanical properties of 3D printed eco-friendly concrete with steel slag. Journal of Building Engineering, 72, 106621. doi:10.1016/j.jobe.2023.106621.

[9] Xu, Z., Zhang, D., Li, H., Sun, X., Zhao, K., & Wang, Y. (2022). Effect of FA and GGBFS on compressive strength, rheology, and printing properties of cement-based 3D printing material. Construction and Building Materials, 339, 127685. doi:10.1016/j.conbuildmat.2022.127685.

[10] Dai, S., Zhu, H., Zhai, M., Wu, Q., Yin, Z., Qian, H., & Hua, S. (2021). Stability of steel slag as fine aggregate and its application in 3D printing materials. Construction and Building Materials, 299, 123938. doi:10.1016/j.conbuildmat.2021.123938.

[11] Liu, J., & Lv, C. (2022). Properties of 3D-Printed Polymer Fiber-Reinforced Mortars: A Review. Polymers, 14(7), 1315. doi:10.3390/polym14071315.

[12] Lesovik, V., Fediuk, R., Amran, M., Alaskhanov, A., Volodchenko, A., Murali, G., Uvarov, V., & Elistratkin, M. (2021). 3D-Printed Mortars with Combined Steel and Polypropylene Fibers. Fibers, 9(12), 79. doi:10.3390/fib9120079.

[13] Ungureanu, D., Onuțu, C., Isopescu, D. N., Țăranu, N., Zghibarcea, Ștefan V., Spiridon, I. A., & Polcovnicu, R. A. (2023). A Novel Approach for 3D Printing Fiber-Reinforced Mortars. Materials, 16(13), 4609. doi:10.3390/ma16134609.

[14] Sukontasukkul, P., Maho, B., Komkham, S., Pianfuengfoo, S., Zhang, H. (Johnson), Yoo, D. Y., Tangchirapat, W., Sae-Long, W., Limkatanyu, S., & Chindaprasirt, P. (2023). Precise determination of initial printable time for cement mortar 3D printing using a derivative method. Rapid Prototyping Journal, 29(9), 1888–1903. doi:10.1108/RPJ-03-2023-0087.

[15] Sukontasukkul, P., Panklum, K., Maho, B., Banthia, N., Jongvivatsakul, P., Imjai, T., Sata, V., Limkatanyu, S., & Chindaprasirt, P. (2022). Effect of synthetic microfiber and viscosity modifier agent on layer deformation, viscosity, and open time of cement mortar for 3D printing application. Construction and Building Materials, 319. doi:10.1016/j.conbuildmat.2021.126111.

[16] Banthia, N., & Gupta, R. (2006). Influence of polypropylene fiber geometry on plastic shrinkage cracking in concrete. Cement and Concrete Research, 36(7), 1263–1267. doi:10.1016/j.cemconres.2006.01.010.

[17] Guerini, V., Conforti, A., Plizzari, G., & Kawashima, S. (2018). Influence of steel and macro-synthetic fibers on concrete properties. Fibers, 6(3), 47. doi:10.3390/fib6030047.

[18] Dai, P., Lyu, Q., Zong, M., & Zhu, P. (2024). Effect of waste plastic fibers on the printability and mechanical properties of 3D-printed cement mortar. Journal of Building Engineering, 83, 108439. doi:10.1016/j.jobe.2024.108439.

[19] Shakor, P., Nejadi, S., & Paul, G. (2019). A study into the effect of different nozzles shapes and fibre-reinforcement in 3D printed mortar. Materials, 12(10), 1708. doi:10.3390/MA12101708.

[20] Kumar Devalla, T., Srinivas, D., Panda, B., & Sitharam, T. G. (2023). Investigation on the flexural and tensile performance of 3D printable cementitious mixtures considering the effect of fiber distribution. Materials Today: Proceedings, 1-6. doi:10.1016/j.matpr.2023.04.081.

[21] Jamnam, S., Maho, B., Techaphatthanakon, A., Ruttanapun, C., Aemlaor, P., Zhang, H., & Sukontasukkul, P. (2022). Effect of graphene oxide nanoparticles on blast load resistance of steel fiber reinforced concrete. Construction and Building Materials, 343, 128139. doi:10.1016/j.conbuildmat.2022.128139.

[22] Panda, B., Chandra Paul, S., & Jen Tan, M. (2017). Anisotropic mechanical performance of 3D printed fiber reinforced sustainable construction material. Materials Letters, 209, 146–149. doi:10.1016/j.matlet.2017.07.123.

[23] Paul, S. C., Tay, Y. W. D., Panda, B., & Tan, M. J. (2018). Fresh and hardened properties of 3D printable cementitious materials for building and construction. Archives of Civil and Mechanical Engineering, 18(1), 311–319. doi:10.1016/j.acme.2017.02.008.

[24] Ding, T., Xiao, J., Zou, S., & Zhou, X. (2020). Anisotropic behavior in bending of 3D printed concrete reinforced with fibers. Composite Structures, 254, 112808. doi:10.1016/j.compstruct.2020.112808.

[25] Ma, G., Zhang, J., Wang, L., Li, Z., & Sun, J. (2018). Mechanical characterization of 3D printed anisotropic cementitious material by the electromechanical transducer. Smart Materials and Structures, 27(7), 75036. doi:10.1088/1361-665X/aac789.

[26] Shi, C., Meyer, C., & Behnood, A. (2008). Utilization of copper slag in cement and concrete. Resources, Conservation and Recycling, 52(10), 1115–1120. doi:10.1016/j.resconrec.2008.06.008.

[27] Scrivener, K. L., & Kirkpatrick, R. J. (2008). Innovation in use and research on cementitious material. Cement and Concrete Research, 38(2), 128–136. doi:10.1016/j.cemconres.2007.09.025.

[28] Li, L. G., Xiao, B. F., Cheng, C. M., Xie, H. Z., & Kwan, A. K. H. (2023). Adding Glass Fibers to 3D Printable Mortar: Effects on Printability and Material Anisotropy. Buildings, 13(9), 2295. doi:10.3390/buildings13092295.

[29] Panda, B., & Tan, M. J. (2018). Material properties of 3D printable high-volume slag cement. Proceedings of the First International Conference on 3D Construction Printing (3DcP) in Conjunction with the 6th International Conference on Innovative Production and Construction (IPC 2018), 26-28 November, Melbourne, Australia.

[30] Shakor, P., Nejadi, S., Paul, G., & Gowripalan, N. (2023). Effects of Different Orientation Angle, Size, Surface Roughness, and Heat Curing on Mechanical Behavior of 3D Printed Cement Mortar With/Without Glass Fiber in Powder-Based 3DP. 3D Printing and Additive Manufacturing, 10(2), 330–355. doi:10.1089/3dp.2021.0067.